High-Frequency Electron Paramagnetic Resonance Studies of VO^{2+} in Low-Temperature Glasses

Devkumar Mustafi,[†] Elena V. Galtseva,[†] J. Krzystek,[‡] Louis-Claude Brunel,[‡] and Marvin W. Makinen*[,†]

Department of Biochemistry and Molecular Biology, The University of Chicago, Cummings Life Science Center, 920 East 58th Street, Chicago, Illinois 60637, and Center for Interdisciplinary Magnetic Resonance, National High Magnetic Field Laboratory, Florida State University, 1800 East Paul Dirac Drive, Tallahassee, Florida 32310

Received: April 20, 1999; In Final Form: October 5, 1999

First-derivative electron paramagnetic resonance (EPR) absorption spectra of the vanadyl ion (VO^{2+}) in glasses of five different organic−aqueous cosolvent mixtures at 10 K are reported over the 9.4−376 GHz microwave frequency range. Whereas absorption features arising from the *g*-parallel and *g*-perpendicular components of the g_e tensor are overlapping at low frequencies, it is shown that they are completely separated at microwave frequencies >110 GHz. The analysis of the EPR spectra revealed that line-broadening is due to *g*-strain over the 9.4−376 GHz range. EPR spectra of VO^{2+} bound to bovine transferrin in a 1:1 molar ratio were also compared at 9.4 and 110 GHz. The results for the VO^{2+}−transferrin complex showed that absorption features corresponding to the *g*-parallel and *g*-perpendicular components of the g_e tensor were similarly separated at high frequency and that line-broadening was attributable to *g*-strain. We show that line-broadening characteristic of *g*-strain under conditions of low *g*-anisotropy can be explained by an $S = {}^1/_2$ spin system in which the principal *g* values are themselves the random variables described by a normal distribution. On this basis, it is shown that line-broadening is proportional to the microwave frequency and the spread of each of the principal values of the g_e tensor.

1. Introduction

The oxovanadium(IV) or vanadyl (VO^{2+}) ion is one of the most stable diatomic ions known, and electron paramagnetic resonance (EPR) absorption of VO^{2+} in condensed phases is observed from cryogenic temperatures to room temperature. There are special advantages in the use of VO^{2+} as an EPR probe of biomolecular structure when compared to other paramagnetic metal ions. VO^{2+} can be substituted for a variety of divalent metal ions in metal-activated enzymes and metalloproteins.[1−9] The free, solvated vanadyl ion, existing as the $[VO(H_2O)_5]^{2+}$ species at low pH, ionizes in the neutral pH region to form an EPR-silent, polymeric $VO(OH)_2$ species, and the EPR signal intensity is proportional only to VO^{2+} bound to nonsolvent ligands or macromolecules in the pH 5−11 region.[10] Consequently, spectra are not complicated in the neutral pH region by equilibria between bound and free species of VO^{2+} with overlapping resonance absorption features.

A major limitation of EPR for probing structural details of a paramagnetic site is the failure to resolve superhyperfine couplings of nearby magnetic nuclei that cause broadening of the EPR absorption through their interaction with the unpaired electron spin. Resolution of hyperfine interactions can be achieved by application of electron nuclear double resonance (ENDOR) spectroscopy, as first demonstrated by Feher,[11] leading to a detailed description of the molecular structure of the paramagnetic site. However, for structure determination by ENDOR, particularly through angle-selected methods,[12−15] *g*-anisotropy in the EPR spectrum can become an important constraint. When *g*-anisotropy is large, the electron spin vector may not be oriented parallel to the applied field, and diagonalization of the hyperfine tensor of ligand nuclei may be difficult. On the other hand, for complexes where *g*-anisotropy is low, the concept of a diagonal hyperfine tensor can be very useful for spectral interpretation. Nonetheless, *g*-anisotropy must be sufficiently large to obtain orientation dependent spectroscopic data.

Because *g*-anisotropy of VO^{2+} is low, there is considerable overlap of the parallel and perpendicular EPR absorption components of VO^{2+} at the usual operating microwave frequencies of commercially available spectrometers. Although VO^{2+} can be employed as a paramagnetic probe for angle-selected ENDOR[15−18] at low microwave frequencies, the overlap of parallel and perpendicular absorption features is restricting, and their complete separation, as could be obtained under high magnetic field conditions, would constitute a decisive advantage for structural analysis. However, high microwave frequencies are expected to lead to line-broadening, a phenomenon known as *g*-strain,[19,20] and broadening may result in decreased resolution. To identify conditions where these opposing effects are not limiting for application of angle-selected ENDOR, we have investigated the spectroscopic behavior of VO^{2+} under high magnetic field conditions in frozen glassy matrices formed from organic−aqueous cosolvent mixtures and in a protein at cryogenic temperatures.

We report here the results of our investigations, showing that there is complete separation of the parallel and perpendicular EPR absorption components of VO^{2+} at microwave frequencies

* Corresponding author. Tel: 773/702-1080. FAX: 773/702−0439. E-mail: m-makinen@uchicago.edu.
[†] University of Chicago.
[‡] Florida State University.

10.1021/jp991287t CCC: $18.00
Published on Web 12/03/1999

>110 GHz and that line-broadening can be considered as essentially due only to *g*-strain for both the $[VO(H_2O)_5]^{2+}$ complex in organic−aqueous cosolvent mixtures and for the VO^{2+} ion bound to the serum transport protein transferrin. Physical mechanisms giving rise to static structural disorder of the inner-shell coordinating ligands are discussed as the origin of *g*-strain, and it is suggested that the extent of *g*-strain for VO^{2+} in a metal ion binding site of a protein may reflect its structure and conformation. The results also indicate that high magnetic fields should provide an incisive advantage for structural analysis with VO^{2+} as the paramagnetic probe through application of angle-selected ENDOR.

2. Experimental Methods

Sample Preparation. Vanadyl sulfate hydrate, anhydrous sodium bicarbonate, methanol, dimethyl sulfoxide (DMSO), *N*,*N*-dimethylformamide (DMF), and 1,10-phenanthroline were purchased as analytical reagents from Aldrich Chemical Co., Inc. (Milwaukee, WI) and were used as received. All solvents were spectroscopic grade (≥99.9%). D_2O (99.8 at. % D) and CD_3OD (99.8 at. % D) were obtained from Cambridge Isotope Laboratories, Inc. (Woburn, MA). Iron-free bovine transferrin (98%) was purchased from Sigma Chemical Company (St. Louis, MO).

Concentrated stock solutions of VO^{2+} were prepared by dissolving vanadyl sulfate hydrate in a small volume of H_2O or D_2O under a nitrogen atmosphere. An aliquot of the stock solution was then diluted with methanol, DMSO or DMF, and water, also under a nitrogen atmosphere, to the final desired concentration, generally 0.01 M in VO^{2+}.

Iron-free bovine transferrin was thrice dialyzed over a period of 24 h against a 0.1 M NaCl solution buffered with 0.02 M HEPES to pH 8.0 containing 10^{-3} M 1,10-phenanthroline. This treatment was followed by exhaustive dialysis against the HEPES/NaCl buffer without 1,10-phenanthroline to remove the metal chelator. The protein concentration was measured spectrophotometrically at 280 nm using 81 000 as the molecular weight and an $E_{1\%}$ value of 11.4.[21] The concentration of vanadyl sulfate was determined gravimetrically or spectrophotometrically at 760 nm using a molar extinction coefficient of 17.6 M^{-1} cm^{-1}.[22,23] Complexes of transferrin with VO^{2+} were prepared by adding the requisite amount of vanadyl sulfate hydrate dissolved in a small quantity of H_2O or D_2O to the protein in 0.1 M NaCl under a nitrogen atmosphere buffered with 0.02 M HEPES to pH 8.0. An aliquot of a $NaHCO_3$ solution was added to a final concentration of 0.01 M. For EPR and ENDOR studies, a protein concentration of $\sim 1.0 \times 10^{-3}$ M was used.

EPR Spectroscopy. High-frequency EPR spectra were recorded with use of a custom-built spectrometer based on an Oxford Instruments Teslatron 17 T superconducting magnet capable of fast field sweeps. As the microwave radiation source, two Gunn oscillators were used operating at 95 or 110 GHz, respectively. Each of the oscillators was equipped with a Schottky diode harmonic generator and a set of appropriate high-pass filters to generate higher frequencies. Details of this apparatus are described elsewhere.[24] The spectrometer was equipped with an Oxford Instruments CF-1200 helium-flow cryostat. Typical conditions for spectral data collection: sample temperature, 10 K; rate of field sweep, 25 mT/min; modulation frequency of the laboratory magnetic field, 8 kHz; modulation amplitude, 0.5 mT. Incident power varied with the operating frequency. The spectrometer was operated without a resonator in a single-pass mode. The detection sensitivity of this configuration has been shown to be of the order of 10^{14} spins mT^{-1} at 300 K and 10^{12} spins mT^{-1} at 5 K with a time constant of 1 s.[24] Calibration of the magnetic field was achieved with use of a powder sample of Mn^{2+} (in MgO) according to the procedure of Burghaus et al.[25]

EPR absorption spectra at X-band were recorded with use of a Bruker ESP 300E spectrometer equipped with a TM_{110} cylindrical cavity, Oxford ESR910 liquid helium cryostat, and ESP 3220 data system, as previously described.[7,18] Typical experimental conditions for X-band EPR measurements: sample temperature, 10 K; microwave frequency, 9.44 GHz; incident microwave power, 64 μW (full power, 640 mW at 0 dB); modulation frequency of the laboratory magnetic field, 12.5 kHz; modulation amplitude, 0.05 mT. The magnetic field was calibrated with use of a small sample of DPPH.

At both X-band and high microwave frequencies, care was taken to ensure that EPR spectra were collected under nonsaturating conditions of the incident microwave power. At 95 and 110 GHz under conditions of high levels of incident microwave power, rapid passage effects were evident in the spectra, comparable to the observations reported by Reijerse and coworkers.[26] At these frequencies reduction of the incident microwave power to levels less than 100 μW was sufficient to avoid these complications. At second and higher harmonics of the fundamental frequencies, rapid passage effects were not observed.

Spectral Simulations. Simulations of EPR spectra collected under X-band and high-frequency conditions were carried out with use of the program WINEPR2.11 (Bruker Instruments, Inc., Billerica, MA) according to second-order perturbation theory. Initial estimates of the spectroscopic parameters ($g_\perp$, $g_\parallel$, $A_\perp$, $A_\parallel$, $\Delta B_\perp$, $\Delta B_\parallel$) were obtained on the basis of visual comparison of the simulated spectrum with the experimental spectrum. The parameters were then refined further by least-squares minimization of calculated and observed spectra in their first-derivative form. On this basis it was found that spectral simulation on the basis of Gaussian functions rather than Lorentzian functions yielded the best fit at all microwave frequencies. When fitting on the basis of superpositioned Gaussian and Lorentzian functions was attempted, the agreement of simulated results with experimental results was invariably less good for values of $\Delta B^{pp}_L/\Delta B^{pp}_G > 0.1$. Consequently, spectral simulations are reported only on the basis of Gaussian functions. Spectral simulations were carried out for conditions of axial symmetry of the g_e and A tensors of the VO^{2+} ion. Within the accuracy of fitting simulated to experimental spectra, we estimated that deviations from axial symmetry less than ± 0.001 in g and $\pm 3.0 \times 10^{-4}$ cm^{-1} in A could not have been detected. These values are within the range of errors associated with experimental determination of these parameters.

3. Results

VO^{2+} in Organic−Aqueous Cosolvent Mixtures. The paramagnetism of VO^{2+} is well behaved, having its origin almost entirely in spin angular momentum. EPR absorption of VO^{2+} is observed over a wide range of temperature and is characterized by axially symmetric g_e and A tensors.[27,28] In frozen solutions at cryogenic temperatures, the powder pattern EPR absorption spectrum of the ($S = {}^1/_2$) VO^{2+} ion is composed of eight parallel and eight perpendicular features due to hyperfine (hf) coupling with the ($I = {}^7/_2$) vanadium nucleus.[27−29]

Figure 1 illustrates the first-derivative EPR absorption spectrum at 9.5 GHz for VO^{2+} in protiated and perdeuterated methanol:water cosolvent mixtures. Although the parallel and perpendicular absorption features overlap, it is seen that the

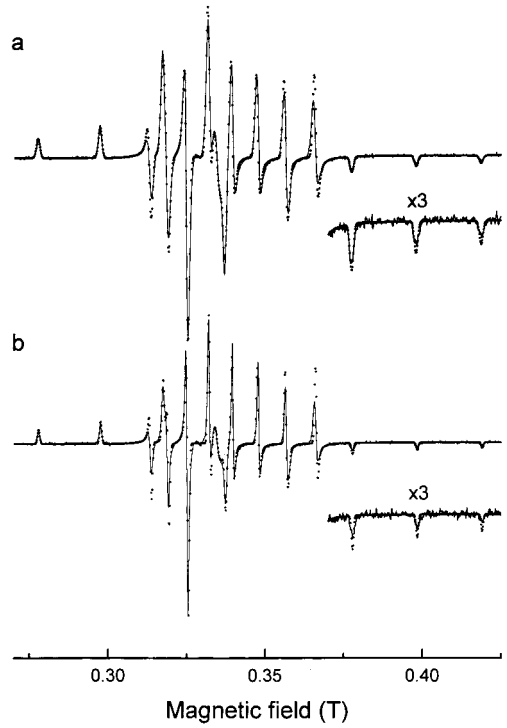

Figure 1. First-derivative EPR absorption spectra of VO^{2+} ion at 9.44 GHz in (a) CH_3OH:H_2O and (b) CD_3OD:D_2O (10:90 v/v) cosolvent mixtures: (solid line) experimental spectrum; (dotted line) simulated spectrum. The final concentration of VO^{2+} was 0.01 M, and the spectra were collected at 10 K.

spectrum is dominated by anisotropy in the vanadium nuclear hf coupling. Comparison of the spectrum of VO^{2+} in the protiated solvent to that in the perdeuterated medium shows that the line width of the $-^3/_2$ perpendicular EPR feature, as the best separated component, decreases, as observed earlier.[15−17] The line widths estimated through spectral simulations in Figure 1 were 1.14 mT for VO^{2+} in the protiated solvent and 0.7 mT in the perdeuterated solvent. From analysis of the X-band continuous wave power saturation curve of VO^{2+} according to Castner,[30] we estimated the value of the inhomogeneity parameter $\Delta B^{pp}{}_L/\Delta B^{pp}{}_G$ to be ~0.016. On this basis, the relaxation determined line width is estimated to be not greater than 0.02 mT. We conclude that the observed line width in Figure 1 must be due primarily to vanadium nuclear hyperfine and unresolved solvent superhyperfine (shf) interactions.

In Figures 2 and 3, we compare EPR spectra of VO^{2+} in a methanol:water (10:90 v/v) cosolvent mixture at four different microwave frequencies. While overlap of parallel and perpendicular absorption features is still evident at 94 GHz, the separation between the highest field perpendicular and the lowest field parallel components becomes complete at frequencies >110 GHz. The lines are considerably broader under high-frequency conditions than observed in Figure 1. The change in the unresolved shf broadening from the protiated solvent compared to that from the perdeuterated solvent could not be detected, showing that it no longer provided a significant contribution to the line width, in contrast to the effect seen in Figure 1. To better understand the physical origins of line-broadening, we have investigated the influence of the matrix of frozen glasses on line-broadening at high frequencies in considerable detail. We have also compared at 9.44 and 110 GHz the line width of VO^{2+} bound to the serum transport protein transferrin.

In addition to the influence of methanol:water cosolvent mixtures illustrated in Figures 2 and 3, we have also examined

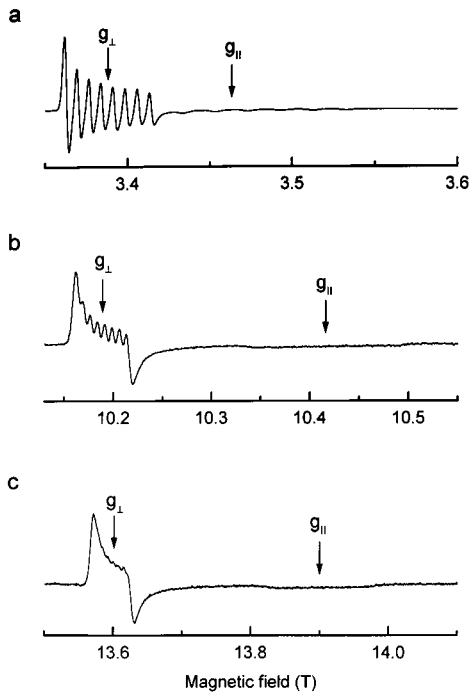

Figure 2. High-frequency EPR spectra of VO^{2+} in CH_3OH:H_2O (10:90 v/v) glass at three different frequencies: (a) 93.57 GHz; (b) 282.10 GHz; (c) 376.62 GHz. The final concentration of VO^{2+} was 0.01 M, and the spectra were collected at 10 K. The approximate positions of the principal components of the g_e tensor are indicated by arrows.

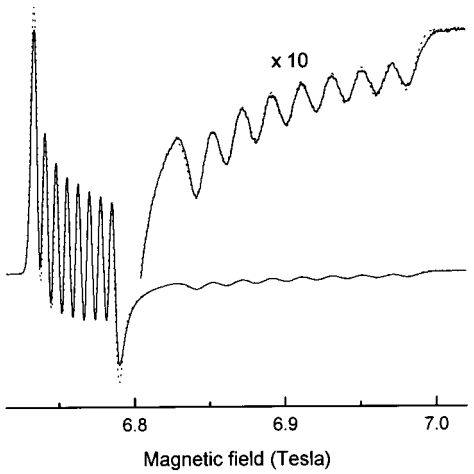

Figure 3. Comparison of experimental and simulated EPR spectra of VO^{2+} in CH_3OH:H_2O (10:90 v/v) at 187.11 GHz: (solid line) experimental spectrum; (dotted line) simulated spectrum. The comparison is provided to indicate the general quality of spectral simulations at high frequencies. In this case, the best least-squares fit was obtained with ΔB^{pp} values of 4.9 mT for perpendicular components and 12.0 mT for parallel components. Other conditions were as in Figure 2.

the influence of DMSO:water and DMF:water cosolvent mixtures, varying the relative amount of each cosolvent. The line widths for VO^{2+} in DMF:water and DMSO:water mixtures were uniformly larger than those in the methanol:water systems. Independent of these observations, we also noticed markedly increased absorption of millimeter and submillimeter radiation by the frozen DMSO:water and DMF:water systems compared to methanol:water, particularly at frequencies ≥326 GHz. We attributed these changes to increased dielectric loss. The limited amount of power reaching the detector under these conditions also resulted in significant deterioration of the signal-to-noise ratio during spectral data collection.

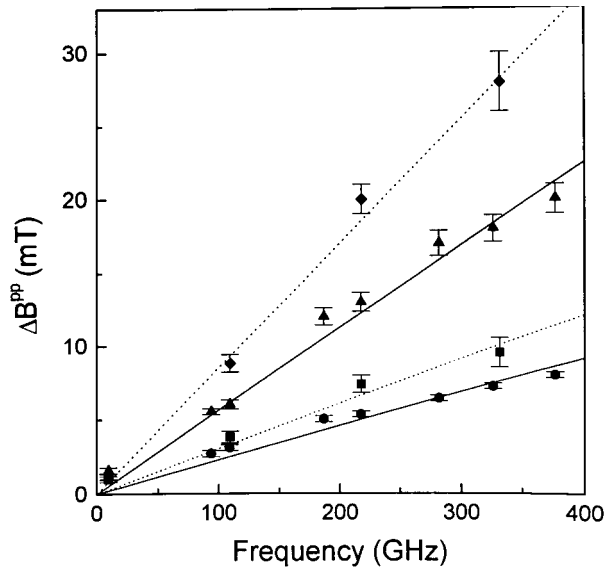

Figure 4. Plots of the parallel and perpendicular EPR absorption components of VO^{2+} in two different solvent mixtures versus operating EPR frequency. The solid lines are for VO^{2+} in CH_3OH:H_2O (10:90 v/v), and the dotted lines are for VO^{2+} in DMF:H_2O (50:50 v/v). Triangles and circles represent the parallel and perpendicular line widths, respectively, for VO^{2+} in CH_3OH:H_2O (10:90 v/v). Diamonds and squares represent the parallel and perpendicular EPR line widths, respectively, for VO^{2+} in DMF:H_2O (50:50 v/v). Line widths were estimated through spectral simulation, as shown in Figures 1 and 3. The straight lines represent linear least-squares fits to the line width estimates at high microwave frequencies only (≥90 GHz) and were not constrained to pass through the origin.

In Figure 4 we have plotted the line widths of parallel and perpendicular absorption features for VO^{2+} in DMF:water (50:50 v/v) and methanol:water (10:90 v/v) cosolvent mixtures, estimated through spectral simulations. The DMF and methanol glass systems exhibited, respectively, the largest and smallest line-broadening influence. The plot illustrates a linear dependence of line width on microwave frequency for both components at high frequencies. The line widths observed for VO^{2+} in DMF:water (90:10) and DMSO:water (50:50 v/v) showed a similar linear dependence, which was intermediate between that exhibited by the two cosolvent mixtures illustrated here.

In Table 1 we have summarized spectroscopic parameters characterizing EPR spectra of VO^{2+} in organic−aqueous cosolvent mixtures, determined through spectral simulations over the 9.44−376.6 GHz range. Under the highest field conditions, the largest line widths of the perpendicular EPR absorption components were estimated to be of the order of 8.0 mT. If we consider this to represent the maximum difference in the field positions of two overlapping absorption components due to g_x and g_y, the detectable upper limit for deviation of the g_e tensor from axial symmetry ($g_x - g_y$) can be no greater than 0.001. Correspondingly, if we assume that the line width of the $+^7/_2$ perpendicular component in the X-band spectrum of VO^{2+} represents the maximum difference between A_x and A_y, the detectable upper limit for deviation of the vanadium hyperfine tensor A from axial symmetry ($A_x - A_y$) is $\leq 3.0 \times 10^{-4}$ cm^{-1}. These limits are within the experimental error associated with determining these parameters. On this basis, we conclude that simulation of spectra under conditions of axial symmetry of the g_e and A tensors is justified.

In Table 1 the principal components of the g_e and A tensors are nearly identical for all five cosolvent mixtures, underlining the internal consistency of the data collected over a wide range of frequency with two different spectrometers. To describe the line-broadening phenomenon illustrated in Figure 4, we have parametrized spectral simulations so as to quantify g-strain. The parameter characteristic of g-strain is labeled σ in Table 1 and is proportional to the slope in Figure 4. Values of $\sigma_{||}$ and $\sigma_\perp$ are correspondingly associated with each set of $g_{||}$ and $g_\perp$ values of VO^{2+} for each cosolvent mixture. The physical origin of σ as a measure of g-strain and static structural disorder will be discussed later.

TABLE 1: Spectroscopic Parameters Characterizing EPR Spectra of VO^{2+} in Organic-Aqueous Cosolvent Mixtures

solvent system	$g_{||}$[a]	$g_\perp$[a]	$\sigma_{||}$[b]	$\sigma_\perp$[b]	$A_{||}$[a]	$A_\perp$[a]
CH_3OH:H_2O (10:90 v/v)	1.934	1.976	0.00144	0.00061	−179.7	−67.4
DMSO:H_2O (90:10 v/v)	1.932	1.973	0.00176	0.00106	−175.0	−64.5
DMSO:H_2O (50:50 v/v)	1.932	1.973	0.00189	0.00102	−175.9	−65.4
DMF:H_2O (90:10 v/v)	1.936	1.975	0.00210	0.00085	−179.0	−66.4
DMF:H_2O (50:50 v/v)	1.936	1.976	0.00221	0.00082	−177.2	−66.4

[a] The principal components of the g and A tensors are defined as $g_{||} = g_{zz}$, $g_\perp = (g_{xx} + g_{yy})/2$ and $A_{||} = A_{zz}$, $A_\perp = (A_{xx} + A_{yy})/2$. Hfc components are given in units of (10^4) cm^{-1}. Uncertainties of ±0.001 in g and of $\pm 3.0 \times 10^{-4}$ cm^{-1} in A were determined by simulation of each EPR spectrum over the microwave frequency range 9.44−376.6 GHz. [b] Values of σ for $g_{||}$ and $g_\perp$ were obtained from the linear dependence of ΔB^{pp} on frequency in the range 9.44−376.6 GHz (cf. Figure 4). The peak-to-peak line widths were determined from spectral simulations. Uncertainties in $\sigma_{||}$ and $\sigma_\perp$ were ±0.00010 and ±0.00005, respectively.

VO^{2+} in Transferrin. Transferrin is a monomeric glycoprotein of approximately 81 000 molecular weight responsible for transport of Fe^{3+} in mammalian blood and exhibits a protein folding pattern of two lobes or domains, each of which contains a metal ion binding site.[31−38] Since the binding sites in each of the two domains exhibit close structural similarity both within the same species of transferrin and among different species of transferrin, functional differences among the members of the transferrin family must be due to variations in the interactions of the two domains with each other dependent upon primary structure.[37,38]

Chasteen and co-workers have characterized the metal ion binding sites with use of VO^{2+} as a paramagnetic probe in the presence of various anionic ligands, showing that the binding of VO^{2+} at each site is essentially stoichiometric.[5,22,23] The two sites, termed A and B, exhibit equivalent metal ion binding affinities and are noninteracting. In binding VO^{2+}, the A and B sites differ slightly according to g and A values. Since the two binding sites exhibit a 0.6 Å root-mean-square displacement of atom pairs between the two domains while having the same set of donor ligand groups from the protein,[38] the differential values of g and A indicate that the electronic structure of VO^{2+} is particularly sensitive to small structural differences.[22,23]

Figure 5 compares the EPR absorption spectra of the VO^{2+} complex of bovine transferrin at 9.44 and 109.9 GHz. Both spectra derive from a solution of the protein to which a 1 molar equiv of VO^{2+} was added followed by addition of HCO_3^-, as described in the Experimental Methods. For human transferrin in the absence of Fe^{3+}, Chasteen and co-workers have demonstrated that VO^{2+} is distributed equally into both A and B binding sites when added to the protein in 1:1 or 1:2 molar equiv.[5] It is seen in the upper part of Figure 5 that the EPR absorptions are each split into two features indicative of two different binding sites. As shown in the X-band spectrum of Figure 5, the A and B sites are better resolved for bovine

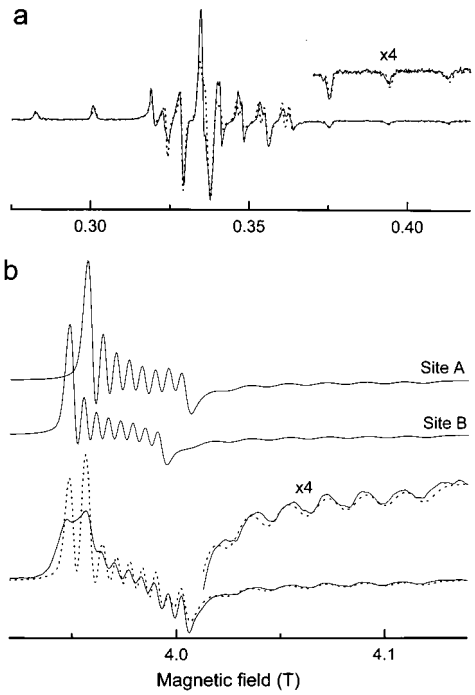

Figure 5. EPR spectra of the VO^{2+}−transferrin (1:1 molar equiv) complex at (a) 9.44 GHz and (b) 109.94 GHz. The final concentration of VO^{2+} was 1×10^{-3} M, and the spectra were collected at 10 K. In the lower panel, the simulated spectra for A and B sites are illustrated separately to show how they differ from the experimental spectrum while there is good agreement between the composite (A + B) spectrum with experiment: (a) (—) experimental spectrum, (···) simulated spectrum; (b) (—) experimental spectrum (the simulated spectra for site A and for site B are illustrated above the experimental spectrum and are labeled *site A* or *site B*, respectively), (···) composite spectrum by addition of spectrum A to spectrum B. It is evident from the diagram that the simulated spectrum of site A or of site B alone cannot account for the observed spectrum. To test for the best fit of the summed spectral contributions of sites A and B to the experimental spectrum, we varied the relative weighting of site A and site B spectra so as to match the composite simulated line width to the observed line width. The summed contributions with weighting site A:site B spectra in either 60:40 or 40:60 ratios produced poor matching to the observed line width while weighting in 55:45 or 45:55 ratios yielded equally good matches to the observed line width but nonetheless less well than 50:50 weighting. We consequently concluded that the best fit was obtained by weighting site A and site B contributions equally.

transferrin in the high-field region under X-band conditions. In contrast, A and B sites are better resolved for human transferrin in the low-field region.[5] These subtle spectral differences are likely to be due to variations in the influence of primary structure on interdomain interactions of the two homologous proteins since the liganding amino acid residues are invariant for different species.[37,38] Demonstration of the splitting of EPR absorption features, nonetheless, clearly shows that two, nonequivalent metal binding sites exist in bovine transferrin as in human transferrin.[5,22]

In Table 2 we have summarized the spectroscopic parameters characterizing the A and B binding sites of VO^{2+} in bovine transferrin estimated on the basis of spectral simulations. While a decrease in the values of $A_{||}$ to -165.0×10^{-4} and -167.0×10^{-4} cm^{-1} for sites A and B, respectively, brought a slightly improved fit for the high-frequency spectrum, the fit to the X-band spectrum suffered noticeably, particularly in the region of the lower field components. Since this decrease in $A_{||}$ is within the error of determining spectral parameters, we concluded that a common set of parameters that produced the best fit to both X-band and high field spectra simultaneously was the best

TABLE 2: Spectroscopic Parameters Characterizing EPR Spectra of the VO^{2+}−Bovine Transferrin Complex

complex	$g_{||}$[a]	$g_{\perp}$[a]	$A_{||}$[a]	$A_{\perp}$[a]	$\Delta B^{pp}{}_{||}$[b]	$\Delta B^{pp}{}_{\perp}$[b]
site A						
VO^{2+}:TFN (1:1)	1.938	1.973	−168.0	−57.5	1.0[c]	1.0[c]
VO^{2+}:TFN (1:1)					9.0[d]	4.5[d]
site B						
VO^{2+}:TFN (1:1)	1.9375	1.978	−170.0	−54.0	1.0[c]	1.0[c]
VO^{2+}:TFN (1:1)					9.0[d]	4.5[d]

[a] The principal components of the g and A tensors are defined as $g_{||} = g_{zz}$, $g_{\perp} = (g_{xx} + g_{yy})/2$ and $A_{||} = A_{zz}$, $A_{\perp} = (A_{xx} + A_{yy})/2$. Hfc components are given in units of (10^4) cm^{-1}. Uncertainties of ±0.001 in g, $\pm 2.5 \times 10^{-4}$ cm^{-1} in $A_{||}$, and $\pm(0.8-1.5) \times 10^{-4}$ cm^{-1} in $A_{\perp}$ were obtained by simulations of EPR spectra at 9.44 and 109.9 GHz. [b] The peak-to-peak EPR line widths for the parallel and perpendicular features are estimated from spectral simulations and are expressed in mT. Uncertainties in line widths were ±0.0003 and ±0.0001 mT for $\Delta B_{||}$ and $\Delta B_{\perp}$, respectively. [c] These parameters are estimated from the EPR spectra of the VO^{2+}:TFN (1:1) complex recorded at 9.44 GHz. [d] These parameters are estimated from the EPR spectra of the VO^{2+}:TFN (1:1) complex recorded at 109.9 GHz.

compromise. Thus, the simulated spectra in Figure 5 are calculated on the basis of the set of parameters for sites A and B in Table 2 which provided the best fit simultaneously to spectra collected at X-band and high-field conditions.

In Figure 5 there is considerably greater discrepancy between simulated and experimental spectra than seen in Figures 1−3. The spectra of VO^{2+} in methanol:water mixtures, however, derive from a collection of essentially homogeneous sites of VO^{2+}, randomly distributed throughout the sample, with each VO^{2+} ion surrounded by an axially symmetric array of chemically identical oxygen-donor ligands.[16] The good agreement between experimental spectra and simulated spectra shows that the physical model of VO^{2+}, as reflected by the parameters in the calculations, accounts adequately for experimental observation. In transferrin the donor ligand groups from the protein, consisting of an aspartyl, two tyrosinyl, and a histidinyl residue, in addition to the bicarbonate ligand, are chemically heterogeneous and must be differentially influenced through domain−domain interactions in view of the observed splitting of spectral features. Also, partitioning of VO^{2+} into two sites may deviate slightly from a strict 50:50 ratio. On this basis, the discrepancies between experimental and simulated spectra in Figure 5 are not unexpected. However, we note that the differences between the composite simulated spectrum and the experimental spectrum can be attributed almost entirely to the relative peak-to-peak amplitudes of the vanadium hf components. Not only does the composite simulated spectrum account well for almost all of the turning points at proper field settings for both high and low microwave frequency conditions, but also such agreement was obtained only within a relatively narrow range of parameter values, i.e., principal components of the g_e and A tensors and line width, that could be fitted to X-band and high-frequency spectra simultaneously. On this basis, we conclude that line width estimates obtained by simulation of VO^{2+}−transferrin spectra in Figure 5 accurately reflect the relative broadening influence of the microwave magnetic field.

4. Discussion

Coordination Environment of VO^{2+} in Organic−Aqueous Cosolvent Mixtures. In purely aqueous solutions at pH < 2.5, VO^{2+} is found as the $[VO(H_2O)_5]^{2+}$ complex in which there are four equatorially positioned H_2O molecules and one axially located H_2O molecule within the inner coordination sphere. We have shown earlier through ^1H and ^{13}C ENDOR studies that

the equatorial positions are occupied only by H_2O molecules in methanol:water mixtures containing greater than 3% (v/v) H_2O, while there is a mixture of complexes having either an H_2O or a CH_3OH molecule in the axial position trans to the vanadyl oxygen.[16] As the H_2O content increases relative to methanol, the axial liganding position in the inner coordination sphere of the VO^{2+} ion becomes increasingly occupied by an H_2O molecule. We can, therefore, conclude that VO^{2+} exists almost entirely in the form of the $[VO(H_2O)_5]^{2+}$ complex with no more than 10% (v/v) methanol in the methanol:water cosolvent mixtures used in this investigation.

Employing comparable ENDOR methodology to characterize the solvent coordination environment of VO^{2+} in DMF:H_2O and DMSO:H_2O mixtures, we have observed resonance features that are characteristic only of equatorial and axial OH groups of water molecules, identical to those observed for the $[VO(H_2O)_5]^{2+}$ complex in methanol:water mixtures, certifying that there are no DMSO or DMF molecules as inner-shell coordinated ligands (D. Mustafi and M. W. Makinen, unpublished observations). Since line-broadening may arise from distortions of the matrix and from alterations in ligand composition and geometry within the inner coordination shell of the metal ion, these observations affirm that the EPR spectra of VO^{2+} ion in the five different cosolvent mixtures employed in this investigation derive only from the $[VO(H_2O)_5]^{2+}$ complex. Therefore, line-broadening, observed as a linear function of the operating microwave frequency illustrated in Figure 4, must have its origin in structural distortions of the inner coordination sphere of VO^{2+} in its $[VO(H_2O)_5]^{2+}$ form induced by the matrix of the frozen (glassy) cosolvent mixture.

We suggest that distortions of the spatial disposition of inner-shell ligands are dependent on the steric accommodation of the VO^{2+} ion with its inner-shell ligands into the spaces created for it in cosolvent mixtures. For the $[VO(H_2O)_5]^{2+}$ complex in methanol:water mixtures, we have demonstrated that outer-shell methanol molecules are hydrogen bonded to inner-shell coordinated OH groups of water molecules through both hydrogen-donor and hydrogen-acceptor relationships.[16] Undoubtedly, H_2O molecules in methanol:water mixtures form comparable geometrical arrangements. On the other hand, DMSO and DMF can form hydrogen bonds with the vanadium-bound H_2O molecules only as hydrogen acceptors. On this basis, it is likely that the $[VO(H_2O)_5]^{2+}$ ion is accommodated more readily into the matrix structure of frozen methanol:water mixtures since both components of the binary organic−aqueous cosolvent mixture can participate in an equivalent manner through hydrogen bonding with inner-shell coordinated H_2O molecules. We conclude that the geometrical arrangement of inner shell H_2O ligands of $[VO(H_2O)_5]^{2+}$ complexes remains more uniform on average since the line-broadening influence of methanol: water mixtures on spectra was less than that observed for DMSO:water and DMF:water mixtures.

Analysis of the Frequency-Dependent Line-Broadening in the EPR Spectra of VO^{2+}. There are several factors that contribute to line-broadening of EPR transitions. Since we maintained identical conditions of temperature and concentration throughout our EPR studies and all data were collected under nonsaturating levels of the incident microwave field, these experimental factors can be excluded as contributing to the increased line widths observed at high frequencies. Magnetic field dependent factors that may contribute to EPR line-broadening are (i) zero-field splitting for systems with $S > {}^1/_2$, (ii) distribution in values of A or A-strain, (iii) spin−lattice relaxation, and (iv) distribution in effective g-factors or g-strain. Since VO^{2+} is characterized by $S = {}^1/_2$, distribution of values of the zero-field parameters D and E, as observed for high-spin Fe^{3+} complexes of proteins,[39] is not operative. Although correlations of g and A values have been noted for VO^{2+} complexes,[3] mechanisms of A-strain underlying line-broadening would be expected to have equivalent contributions for each cosolvent environment in Figures 1−4 since the inner coordination sphere corresponds only to that of the $[VO(H_2O)_5]^{2+}$ ion. Froncisz and Hyde observed an m_I dependence of line width together with g-strain in EPR spectra of square-planar Cu^{2+} complexes in glassy matrices in the microwave frequency range of 2−9 GHz.[40] In the frequency range of our studies, no m_I dependence on microwave frequency could be established in EPR spectra of VO^{2+} within the quantitative limits stated for analysis of spectra through simulations. Effects of T_1 relaxation on line-broadening can be ruled out since we have shown that this cannot be an important contribution to the line width at X-band. Also, the linear relationships illustrated in Figure 4 demonstrate that the contribution of this effect is negligible, if any. On this basis, we assign the effect illustrated in Figure 4 to g-strain, a term first introduced by Anderson and co-workers[20] to describe the broadening mechanism observed in EPR that is linearly dependent on microwave frequency or magnetic field.

We have pointed out above that the 10:90 (v/v) methanol: water glass was associated with the narrowest line widths while the line widths observed for VO^{2+} in DMF:water or DMSO: water mixtures were broader. Since the inner coordination sphere of VO^{2+} is comprised by five water molecules in all five cosolvent mixtures, corresponding to the $[VO(H_2O)_5]^{2+}$ complex, we assume that the ligands to the metal ion become structurally disordered because of perturbations induced by the matrix upon freezing. The degree of structural disorder is proportional to the extent of g-strain. As shown through Table 1, a quantitative estimate of the extent of g-strain is given by σ, and we invoke this parameter as a measure of the influence of static structural disorder on line-broadening observed in experimental spectra.

To gain insight into the origins of g-strain, as defined by the values of σ in Table 1, we replace the concept of a single spin system with a unique g_e tensor by an ensemble of spin systems, each with a slightly different g_e tensor, following the description of the statistical model of g-strain developed by Hagen and co-workers.[41−44] The position of a resonance line is defined by the spectroscopic splitting factor in eq 1, where $i = \{x, y, z\}$

$$g = \left[\sum_{i=1}^{3} l_i^2 g_i^2\right]^{1/2} \tag{1}$$

represents the principal axes of g_e and the l_i are the corresponding direction cosines with respect to **B**. In the absence of hf coupling, the effective resonance condition is given by eq 2 for

$$B = \frac{h\nu}{\beta g} \tag{2}$$

an $S = {}^1/_2$ spin system. With respect to eq 2 we assume that the principal g values are themselves the random variables, each being described by a normal distribution, as given in eq 3, where

$$f(g_i) = \frac{1}{(\sqrt{2\pi})\sigma_i} \exp\left[-\frac{(g_i - \bar{g}_i)^2}{2\sigma_i^2}\right] \tag{3}$$

$f(g_i)$ is a probability density, $\bar{g}_i$ is the mean value of g_i, and σ_i is the standard deviation of g_i. Although the distribution of each

g_i according to eq 3 is symmetric in g space, the corresponding distribution of the magnetic field is asymmetric in **B** space.[44,45] However, it is straightforward to show that there is a normal distribution of the magnetic field, given by eq 4, under the

$$f(B_i) = \frac{1}{(\sqrt{\pi/2})\Delta_i} \exp\left[-\frac{2(B_i - \bar{B}_i)^2}{\Delta_i^2}\right] \quad (4)$$

condition of low g-anisotropy with $\sigma_i \ll g_i$ where $\bar{B}_i = h\nu/\beta\ \bar{g}_i$ and $\Delta_i = 2h\nu\sigma_i/\beta\ \bar{g}_i^2$. As seen in Table 1, the condition of low g-anisotropy with $\sigma_i \ll g_i$ applies to VO^{2+}.

From Figure 1 it is evident that the only prominent contributions to line width at low frequencies are hf coupling due to the vanadium nucleus and shf coupling of solvent hydrogens. As pointed out in the Results, these contributions to the line width are best described by Gaussian functions. Therefore, at all microwave frequencies, when g-strain is taken into account, the spectrum of the ensemble of spin systems remains Gaussian for a given orientation of **B** with peak-to-peak width given by eq 5, where the Δ's represent the individual line width

$$[\Delta B^{pp}(\nu)]^2 = \Delta_{hf}^2 + \Delta_{shf}^2 + \Delta(\nu)^2 \quad (5)$$

contributions due to vanadium hf coupling, solvent hydrogen shf coupling, and variation in g values or g-strain, respectively.[46,47]

At high frequencies ($\geq$90 GHz), the line width contribution due to g-strain dominates [$\Delta_{hf}^2 + \Delta_{shf}^2 \ll \Delta(\nu)^2$], as is evident in Figure 4, and an absorption line of the ensemble now reflects to first order a normal distribution of the magnetic fields, which can be represented by a Gaussian line positioned at $\bar{B}$ of peak-to-peak width Δ. This leads to the relationship in eq 6, through

$$\Delta B_i^{pp} = \frac{h\nu}{\beta}\frac{2\sigma_i}{(\bar{g}_i^2 - \sigma_i^2)} \approx \frac{h\nu}{\beta}\frac{2\sigma_i}{\bar{g}_i^2} \quad (6)$$

which we see that the peak-to-peak width of the line is linearly dependent on the microwave frequency and proportional to the magnitude of σ_i. On this basis, σ_i is a direct measure of the distribution of the values of g_i about its mean value. Thus, eq 6 provides the basis for extracting values of σ from results such as those plotted in Figure 4, and the values of σ listed in Table 1 were calculated by applying eq 6 to the slopes in Figure 4.

Whereas the contribution of g-strain to line-broadening is dominant at high microwave frequencies, the contribution at low frequencies ($\leq$9 GHz) is essentially negligible [$\Delta_{hf}^2 + \Delta_{shf}^2 \gg \Delta(\nu)^2$]. As seen in Figure 4, the observed line width at 9.4 GHz deviates from the strict linear behavior that is dictated by line width estimates at high frequencies. In the low-frequency regime, the line width has become independent of microwave frequency and is determined by other mechanisms, namely, vanadium hf coupling and solvent hydrogen shf coupling interactions, as pointed out in the Results.

In Table 2, we have summarized the EPR spectroscopic parameters of the VO^{2+} complex of bovine transferrin. Values of the principal components of the g_e and A tensors and the peak-to-peak EPR line widths are compared for spectra at microwave frequencies of 9.44 and 109.9 GHz. Values of the g and A components for A and B sites, as listed in Table 2, are in good agreement with those reported by Chasteen and coworkers for human transferrin.[5,22,23] Most importantly, the increase in EPR line widths of the VO^{2+}−transferrin complex at 109.9 GHz over that observed at 9.44 GHz, as seen in Table 2, is comparable to the increase observed for both g-parallel and g-perpendicular components of VO^{2+} in organic−aqueous cosolvent mixtures. These results, thus, demonstrate that the liganding amino acid side chain environment of VO^{2+} in transferrin has not altered the mechanism of line-broadening, for instance, through covalent effects with A-strain. The dependence of line-broadening of VO^{2+} in transferrin on microwave frequency is due to g-strain as for VO^{2+} in frozen glassy matrices.

Since the origin of g-strain for VO^{2+} is static structural disorder both in cosolvent mixtures and in the protein, it is of interest to consider how the disorder differs between the two types of systems. Static structural disorder of VO^{2+} sites in cosolvent mixtures arises from perturbations of the glass-forming solvent on the inner-sphere ligands of the metal ion. On the other hand, structural disorder in metal ion binding sites in proteins arises from dynamical fluctuations associated with conformational substates of the protein that are transmitted to the metal ion through coordinating ligands and are "frozen in" at cryogenic temperatures. These conformational substates are similar to each other in potential energy and contribute to the dynamical fluctuations of the macromolecule at normal temperatures.[48] Since effects of physical or chemical processes such as ligand binding, changes in pH, or allosteric interactions, for instance, when transmitted through the protein, influence the distribution and extent of conformational substates, changes in the dynamical structure of proteins may be reflected through variations in the extent of g-strain. Comparison of the line-broadening of a paramagnetic metalloprotein prepared in different ligand-bound or functional states should then give rise to behavior comparable to that observed in Figure 4, whereby the slope of the ΔB^{pp} vs microwave frequency plot may be characteristic of the functional or ligand-bound state of the protein.

The discussion outlined above leads to the suggestion that the extent of g-strain exhibited by the $[VO(H_2O)_5]^{2+}$ ion in frozen organic−aqueous matrices reflects the degree to which the metal ion with its inner-shell ligands fills the space created for it through proton-donor and proton-acceptor hydrogen bonding relationships. Similarly, changes in the distribution of conformational substates of a protein through chemical or physical processes may alter the degree to which the VO^{2+} ion and its immediate inner-shell coordinating ligands fill the space available to it in a metal ion binding site. The degree to which molecules fill the space available to them in liquids and solids is known as the packing density[49] and is a basic physical property characterizing their static accessibility. Stapleton and co-workers[50−52] have suggested that a fractal dimensionality estimated from the temperature dependence of the spin−lattice relaxation rate of low-spin ferric heme proteins at cryogenic temperatures is a quantitative measure of the degree to which a structure, in this case a ferric−porphyrin complex, fills the space in which it resides. Correspondingly, the extent of g-strain may reflect the degree to which the VO^{2+} ion with its inner-shell ligands fills the space provided within its immediate environment according to van der Waals relationships for steric accessibility. Since instrumentation for high-field electron magnetic resonance experiments, such as that described in this report, has become more generally available, it would be of considerable interest to determine the extent to which such differences in g-strain can be observed and whether they can be related to the underlying atomic structure of the protein.

Acknowledgment. We thank Professor A. Angerhofer for special assistance in measurements of relaxation properties of VO^{2+} in organic−aqueous glasses with a Bruker Elexsys 580

pulsed spectrometer and for helpful discussions. This work was supported by grants from the National Science Foundation (MCB-9513858), the National Institutes of Health (GM21900), the Human Frontier Science Program (RG-349/94), the National High Magnetic Field Laboratory, and the National High Magnetic Field Laboratory User Program.

References and Notes

(1) Chasteen, N. D. *Coord. Chem. Rev.* **1977**, *22*, 1.
(2) Chasteen, N. D. *Struct. Bonding* **1983**, *53*, 105.
(3) Chasteen, N. D. In *Biological Magnetic Resonance*; Berliner, L. J., Reuben, J., Eds.; Plenum: New York, 1981; Vol. 3, pp 53−119,.
(4) Chasteen, N. D.; DeKoch, R. J.; Rogers, B. L.; Hanna, M. W. *J. Am. Chem. Soc.* **1973**, *95*, 1301.
(5) White, L. K.; Chasteen, N. D. *J. Phys. Chem.* **1979**, *83*, 279.
(6) DeKoch, R. J.; West, D. J.; Cannon, J. C.; Chasteen, N. D. *Biochemistry* **1974**, *13*, 4347
(7) Mustafi, D.; Nakagawa, Y. *Proc. Natl. Acad. Sci. U.S.A.* **1994**, *91*, 11323.
(8) Mustafi, D.; Nakagawa, Y. *Biochemistry* **1996**, *35*, 14703.
(9) Banerjee, A.; Chen, S.; Ruetthard, H.; Jiang, F.; Huang, V. W.; Sprinzl, M.; Makinen, M. W. In *Vanadium Compounds: Chemistry Biochemistry and Therapeutic applications*; Tracy, A. S., Crans, D. C., Eds.; ACS Symposium Series No. 711; American Chemical Society: Washington, DC, 1998; pp 104−116.
(10) Francavilla, J.; Chasteen, N. D. *Inorg. Chem.* **1975**, *14*, 2860.
(11) Feher, G. *Phys. Rev.* **1956**, *103*, 834.
(12) Rist, G.; Hyde, J. S. *J. Chem. Phys.* **1968**, *49*, 2449.
(13) Hoffman, B. M.; Martinsen, J.; Venters, R. A. *J. Magn. Reson.* **1984**, *59*, 110.
(14) Hurst, G. C.; Henderson, T. A.; Kreilick, R. W. *J. Am. Chem. Soc.* **1985**, *107*, 7294.
(15) Makinen, M. W.; Mustafi, D. In *Metal Ions in Biological Systems*; Sigel, H.; Sigel, A., Eds; Mercel Dekker: New York, 1995; Vol. 31, pp 89−127.
(16) Mustafi, D.; Makinen, M. W. *Inorg. Chem.* **1988**, *27*, 3360.
(17) Mustafi, D.; Telser, J.; Makinen, M. W. *J. Am. Chem. Soc.* **1992**, *114*, 6219.
(18) Jiang, F. S.; Makinen, M. W. *Inorg. Chem.* **1995**, *34*, 1736.
(19) Pilbrow, J. R. *Transition Ion Electron Paramagnetic Resonance*; Clarendon Press: Oxford, U.K., 1990; Chapter 5, pp 211−259.
(20) Anderson, R. E.; Dunham, W. R.; Sands, R. H.; Bearden, A. J.; Crespi, H. L. *Biochim. Biophys. Acta* **1975**, *408*, 306.
(21) Aisen, P.; Aasa, R.; Malmstrom, B. G.; Vanngard, T. *J. Biol. Chem.* **1967**, *242*, 2484.
(22) Cannon, J. C.; Chasteen, N. D. *Biochemistry* **1975**, *14*, 4573.
(23) Chasteen, N. D.; White, L. K.; Campbell, R. F. *Biochemistry* **1977**, *16*, 363.
(24) Hassan, A.; Pardi, L. A.; Krzystek, J.; Sienkiewicz, A.; Goy, P.; Rohrer, M.; Brunel, L. C. *J. Magn. Reson*., in press.
(25) Burghaus, O.; Plato, M.; Rohrer, M.; Möbius, K.; MacMillan, F.; Lubitz, W. *J. Phys. Chem.* **1993**, *97*, 7639.
(26) van Dam, P. J.; Reijerse, E. J.; Klaasen, A. A. K.; Boonman, M. E. J.; van Bentum, P. J. M.; Perenboom, J. A. A. J.; Hagen, W. R. In *Metal Ions in Biology and Medicine*; Collery, Ph., Corbello, J., Domingo, J. L., Etienne, J. C., Llobet, J. M., Libbey, J., Eds.; Eurotext: Paris, 1996; Vol. 4, pp 27−29.
(27) Gersman, H. R.; Swalen, J. D. *J. Chem. Phys.* **1962**, *36*, 3221.
(28) Kivelson, D.; Lee, S. K. *J. Chem. Phys.* **1964**, *41*, 1896.
(29) Albanese, N. F.; Chasteen, N. D. *J. Phys. Chem.* **1978**, *82*, 910.
(30) Castner, T. G., Jr. *Phys. Rev.* **1959**, *115*, 1506.
(31) Bates, G. W.; Schlabach, M. R. *J. Biol. Chem.* **1973**, *248*, 3228.
(32) Harris, D. C.; Aisen, P. *Biochemistry* **1975**, *14*, 262.
(33) Schlabach, M. R.; Bates, G. W. *J. Biol. Chem.* **1975**, *250*, 2182.
(34) MacGillivray, R. T. A.; Moore, S. A.; Chen, J.; Anderson, B. F.; Baker, H.; Luo, Y.; Bewley, M.; Smith, C. A.; Murphy, M. E. P.; Wang, Y.; Mason, A. B.; Woodworth, R. C.; Brayer, G. D.; Baker, E. N. *Biochemistry* **1998**, *37*, 7919.
(35) Moore, S. A.; Anderson, B. F.; Groom, C. R.; Haridas, M.; Baker, E. N. *J. Mol. Biol.* **1997**, *274*, 222.
(36) Anderson, B. F.; Baker, H. M.; Dodson, E. J.; Norris, G. E.; Rumball, S. V.; Waters, J. M.; Baker, E. N. *Proc. Natl. Acad. Sci. U.S.A.* **1987**, *84*, 1769.
(37) Bailey, S.; Evans, R. W.; Garratt, R. C.; Gorinsky, B.; Hasnain, S.; Horsburgh, C.; Jhoti, H.; Lindley, P. F.; Mydin, A.; Sarra, R.; Watson, J. L. *Biochemistry* **1988**, *27*, 5804.
(38) Baker, E. N.; Lindley, P. F. *J. Inorg. Biochem.* **1992**, *47*, 147.
(39) Gaffney, B. J.; Maguire, B. C.; Weber, R. T.; Maresch, G. G. *Appl. Magn. Reson.* **1998**, *16*, 207.
(40) Froncisz, W.; Hyde, J. S. *J. Chem. Phys.* **1980**, *73*, 3123.
(41) Hagen, W. R. *J. Magn. Reson.* **1981**, *44*, 447.
(42) Hagen, W. R.; Hearshen, D. O.; Sands, R. H.; Dunham, W. R. *J. Magn. Reson.* **1985**, *61*, 220.
(43) Hagen, W. R.; Hearshen, D. O.; Sands, R. H.; Dunham, W. R. *J. Magn. Reson.* **1985**, *61*, 233.
(44) Strong, L. H. Biophysical Studies on Selected Iron-Sulfur Proteins. Ph.D. Dissertation, University of Michigan: Ann Arbor, Michigan, 1976; p 277.
(45) Aasa, R.; Vanngård, T. *J. Magn. Reson.* **1975**, *19*, 308.
(46) Hughes, D.; McDonald, D. *Proc. Phys. Soc.* **1961**, *78*, 75.
(47) Dobryakov, S. N.; Lebedev, Ya. S. *Dokl. Akad. Nauk SSSR* **1968**, *182*, 68.
(48) Frauenfelder, H.; Sligar, S. G.; Wolynes, P. G. *Science* **1991**, *254*, 1598.
(49) Bondi, A. *J. Phys. Chem.* **1964**, *68*, 441−451.
(50) Stapleton, H. J.; Allen, J. P.; Flynn, C. P.; Stinson, D. G.; Kurtz, S. R. *Phys. Rev. Lett.* **1980**, *45*, 1456.
(51) Allen, J. P.; Colvin, J. T.; Stinson, D. G.; Flynn, C. P.; Stapleton, H. J. *Biophys. J.* ***1982***, 38, 299.
(52) Colvin, J. T.; Stapleton, H. J. *J. Chem. Phys.* **1985**, *82*, 4699.